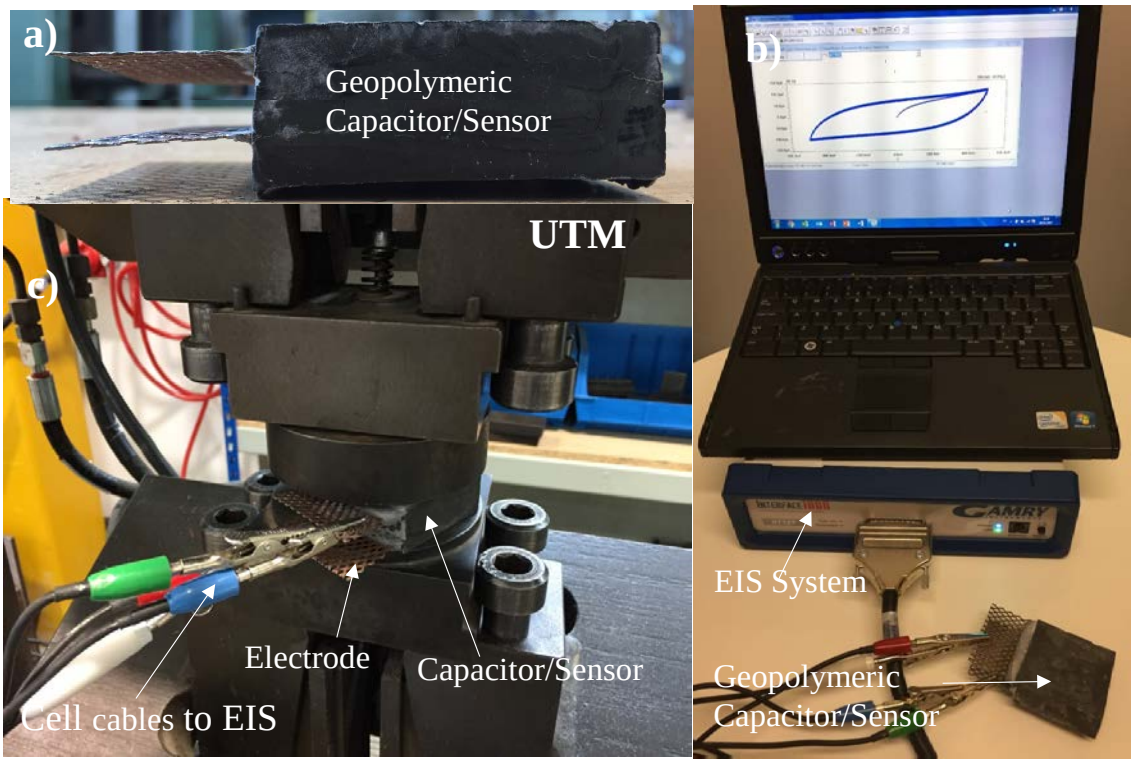

Fig. 1. Experimental setup. a) KGP capacitor/sensor with electrodes, b) EIS characterization of the KGP capacitors, c) EIS characterization of the KGP sensors under load.

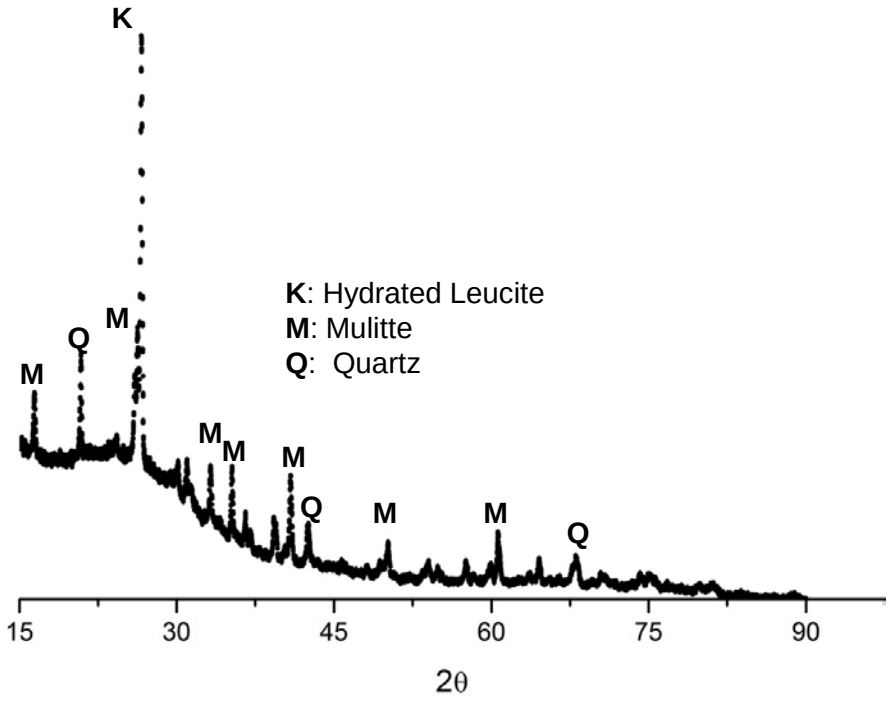

Fig. 2. XRD pattern for the KGP cementitious composite

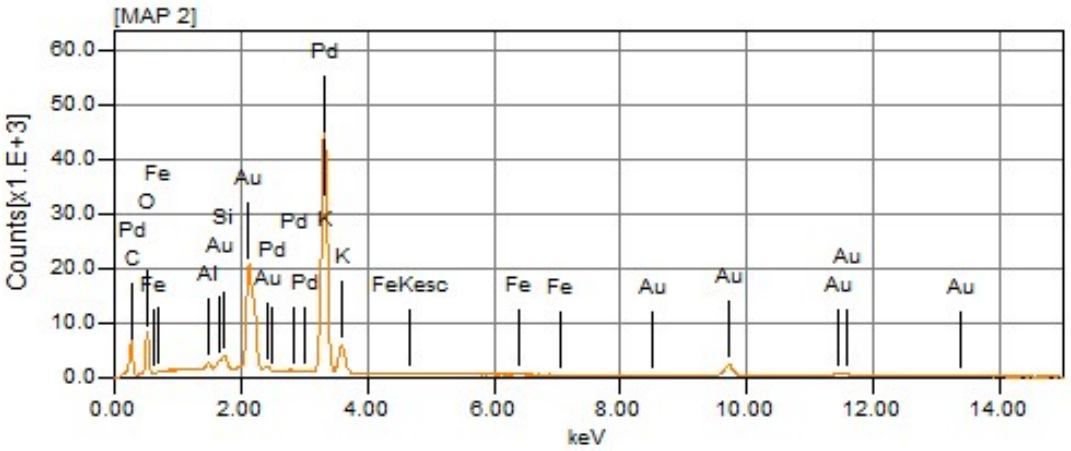

Fig. 3. EDX spectrum for the KGP cementitious composite

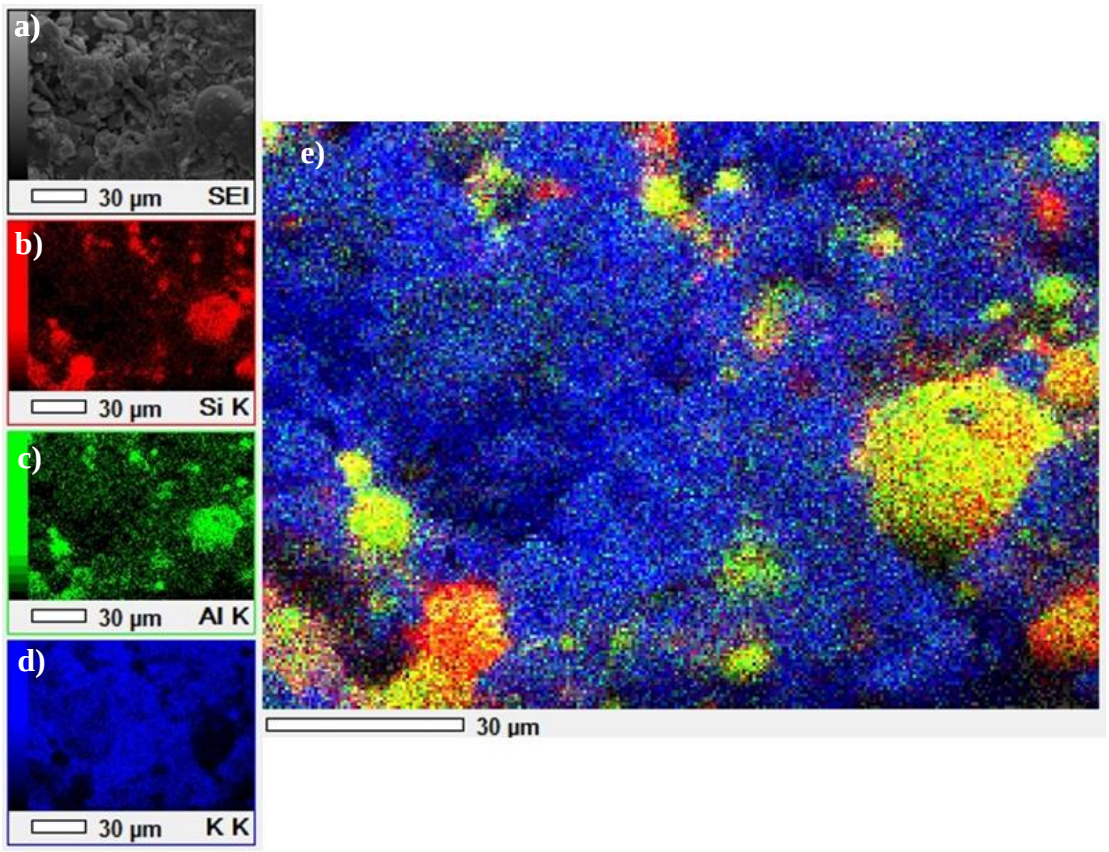

Fig.4. EDX element maps for the KGP cementitious composite. a) SEM image of the KGP cementitious composite, b) Si element map, c) Al element map, d) K element map, e) element map combining Si, Al and K.

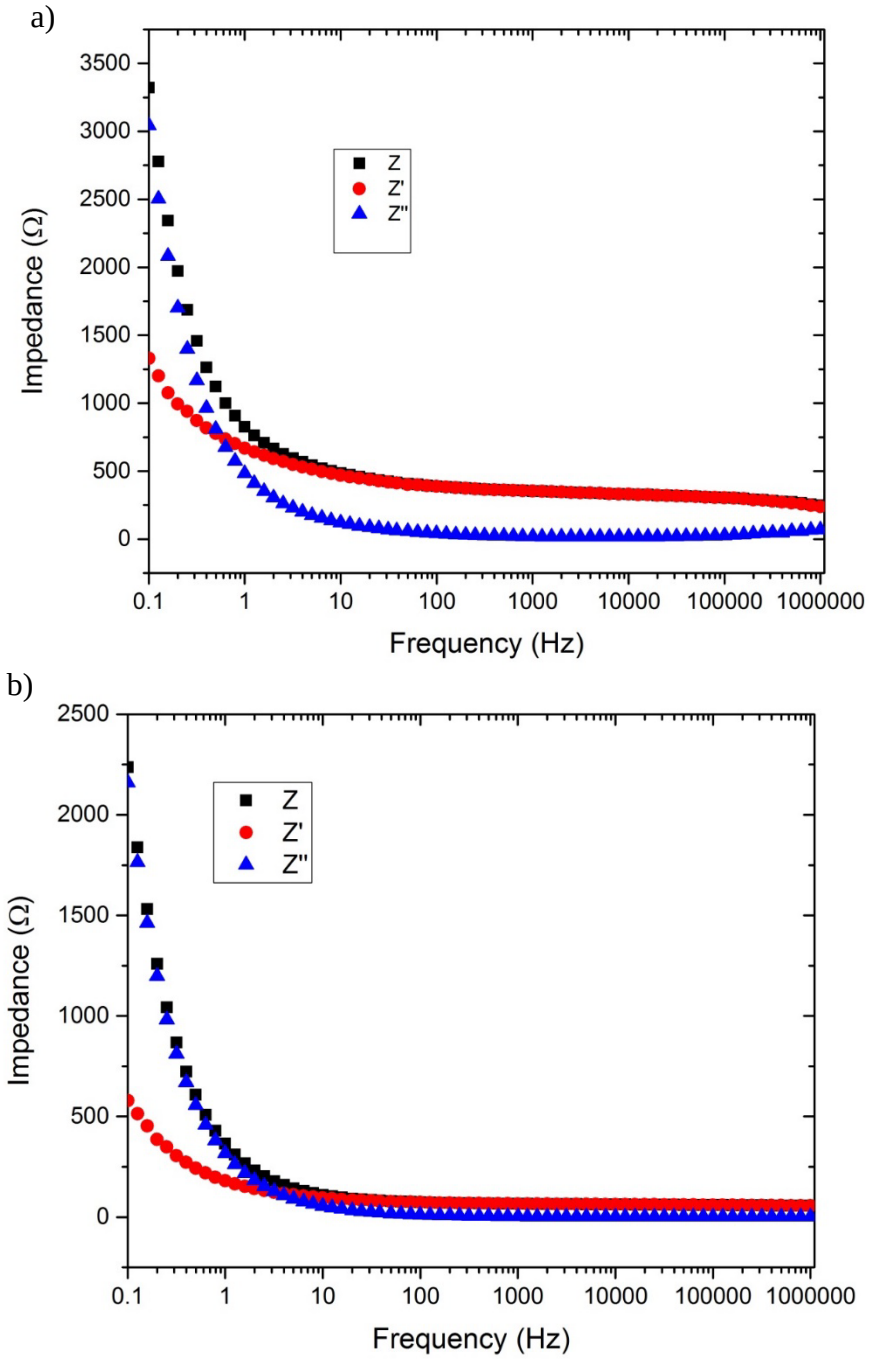

Fig. 5. Bode plot of the impedance for the KGP capacitors/sensors at room temperature. a) capacitor/sensor 1, b) capacitor/sensor 2.

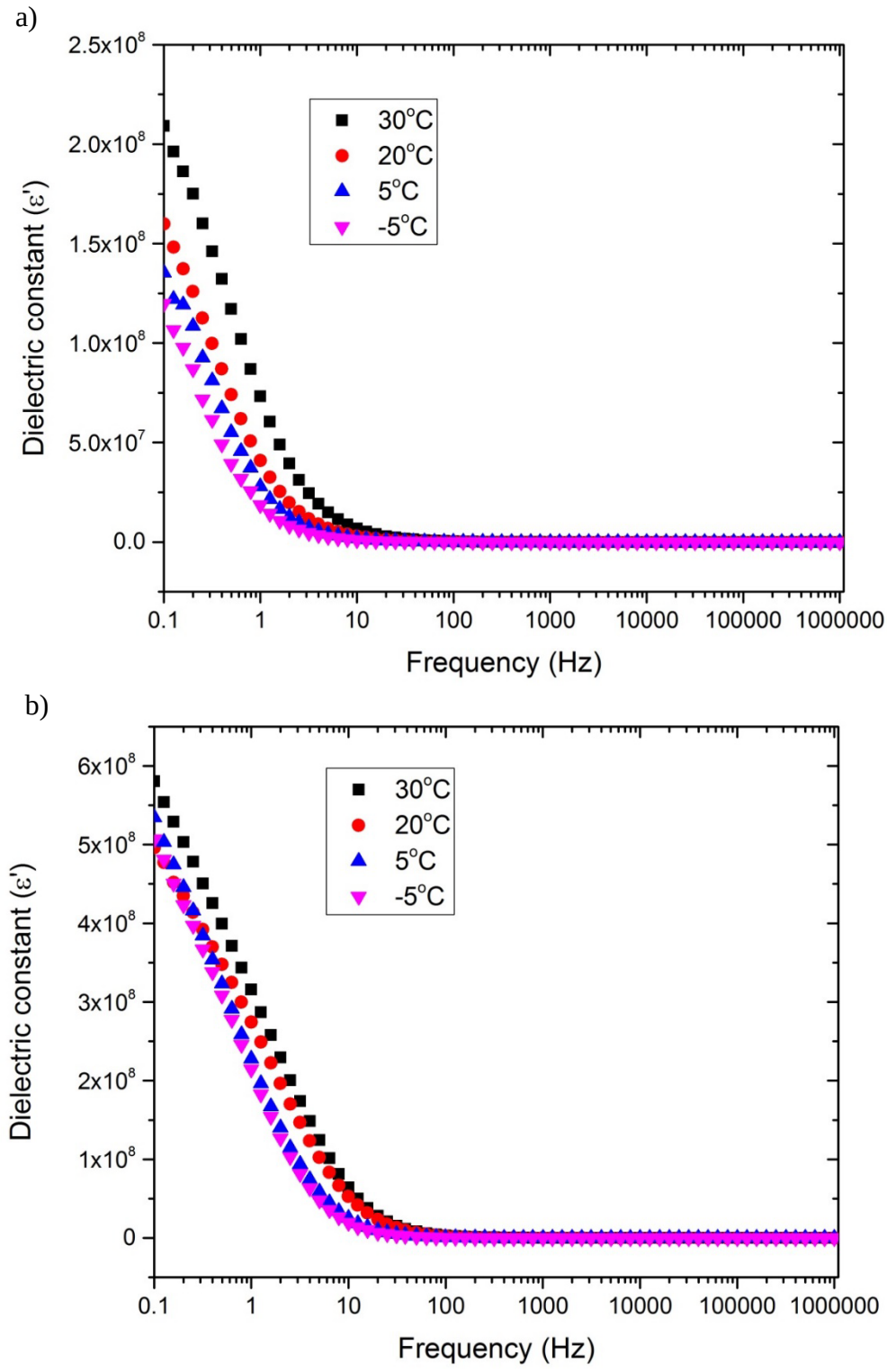

Fig. 6. Dielectric constant of the KGP capacitors/sensors at different temperatures. a) capacitor/sensor 1, b) capacitor/sensor 2

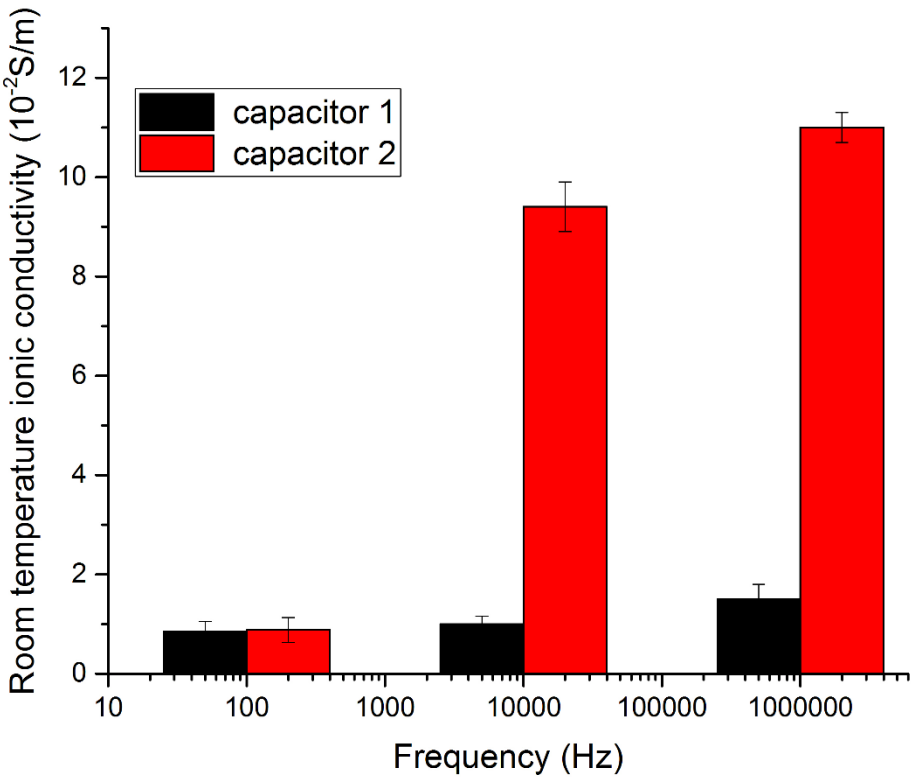

Fig. 7. Ionic conductivity of KGP capacitors/sensors at room temperature

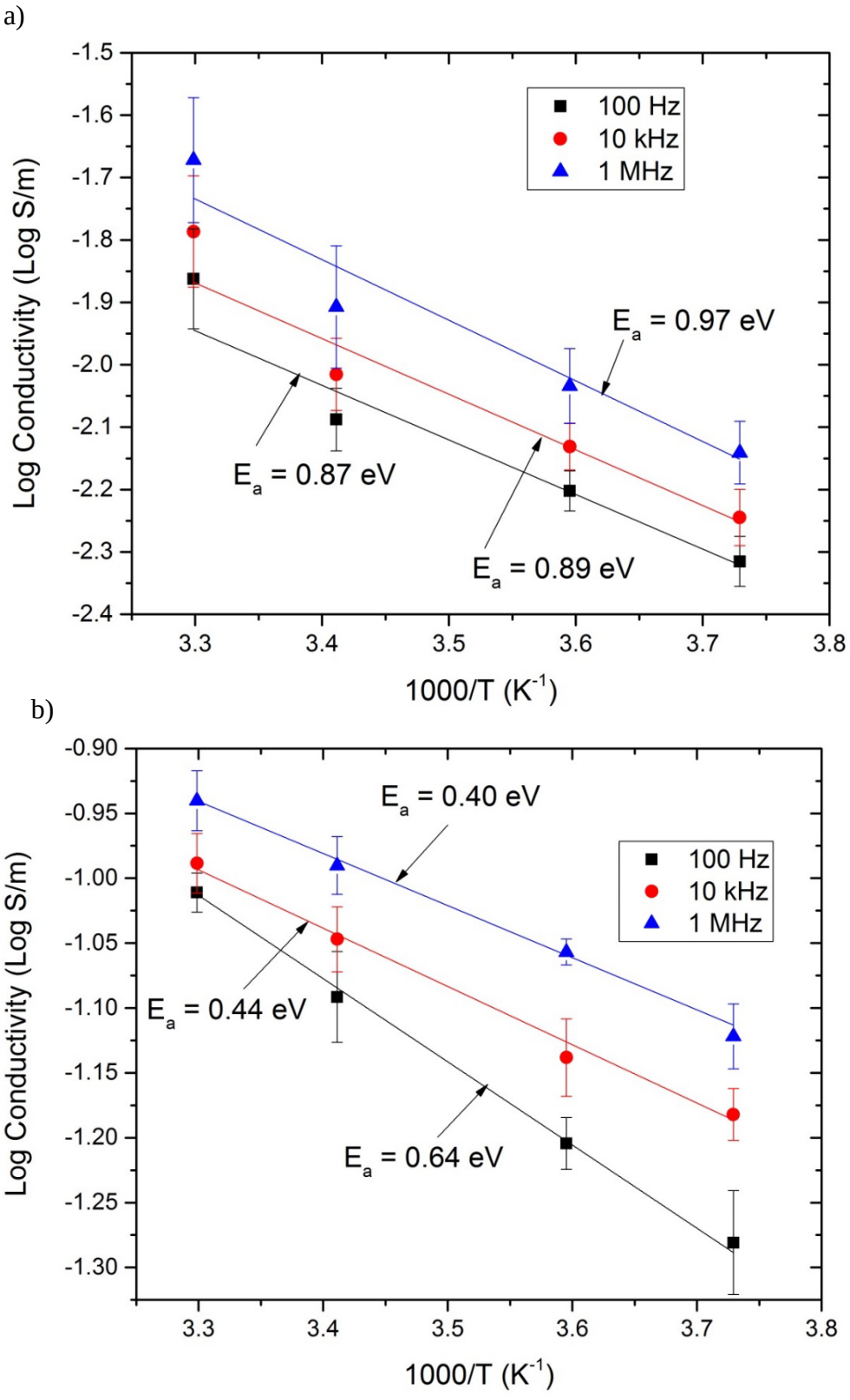

Fig. 8. Arrhenius plot of the ac-conductivity for the KGP capacitors/sensors at different frequencies. a) capacitor/sensor 1, b) capacitor/sensor 2

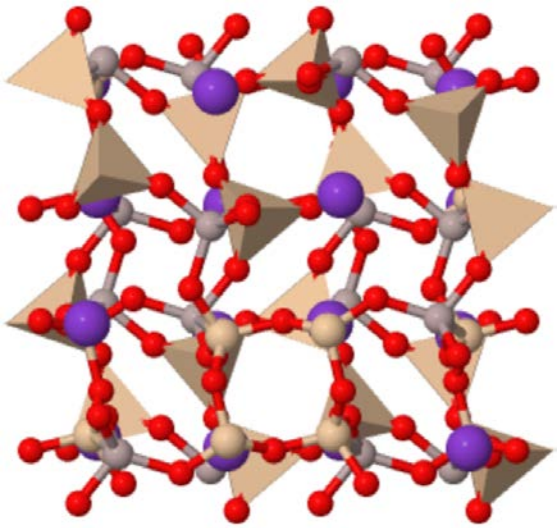

Fig.9. A three-dimensional framework of $[SiO_4/AlO_4]^-$ tetrahedral of leucite-type KGP cementitious composite . The silver atoms are aluminum, the red oxygen, the desert sand atoms are silica and the purple atoms are potassium. The Space group is I 41/a, tetragonal structure with a = 13. 090 Å, b =13.090 Å, c =13.750 Å.

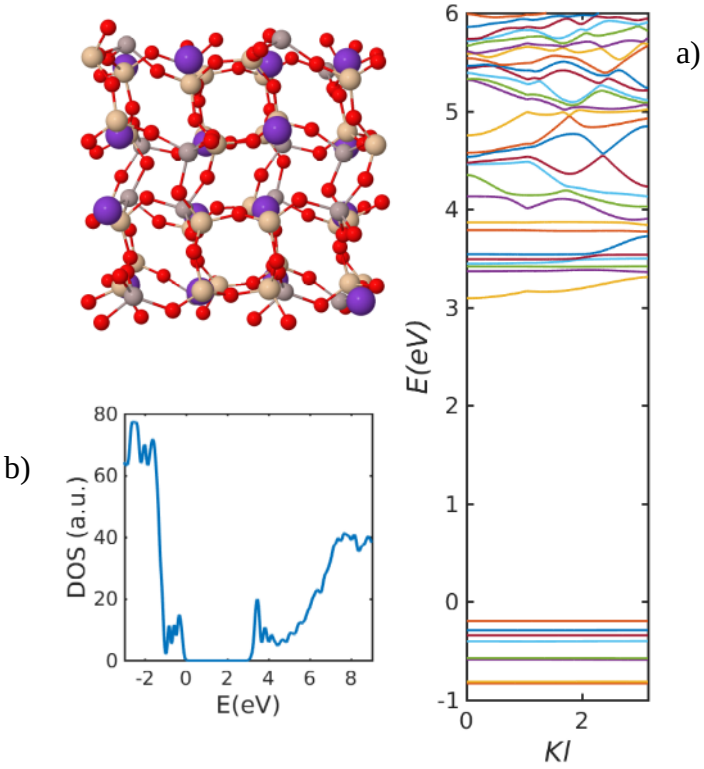

Fig. 10: a) Energy band structure of the KGP cementitious composite, b) density of states (DOS) of the KGP composite.

a)

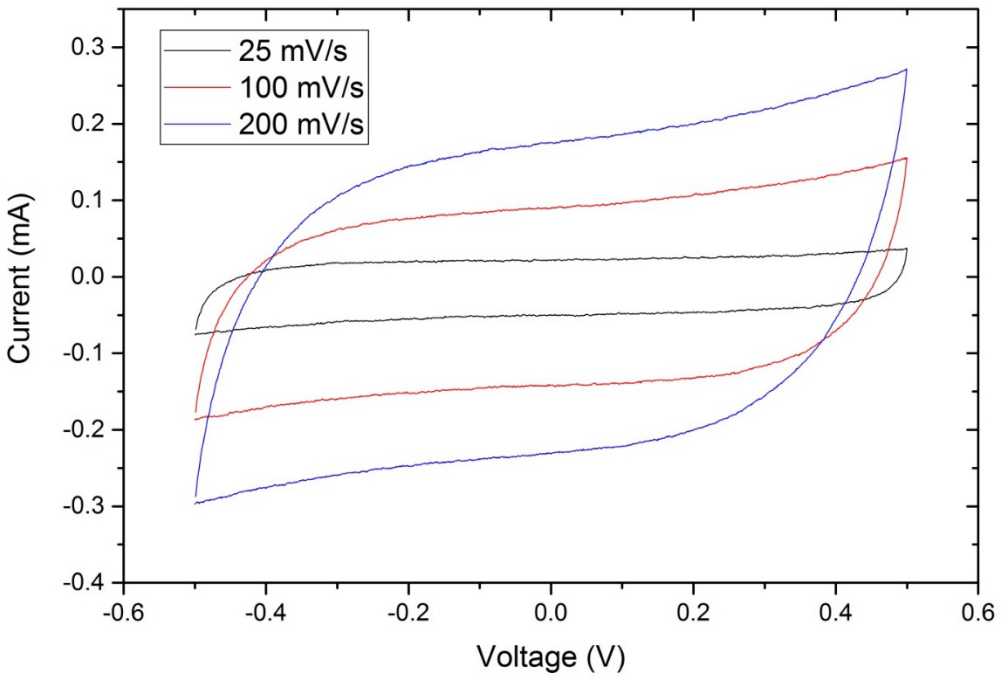

b)

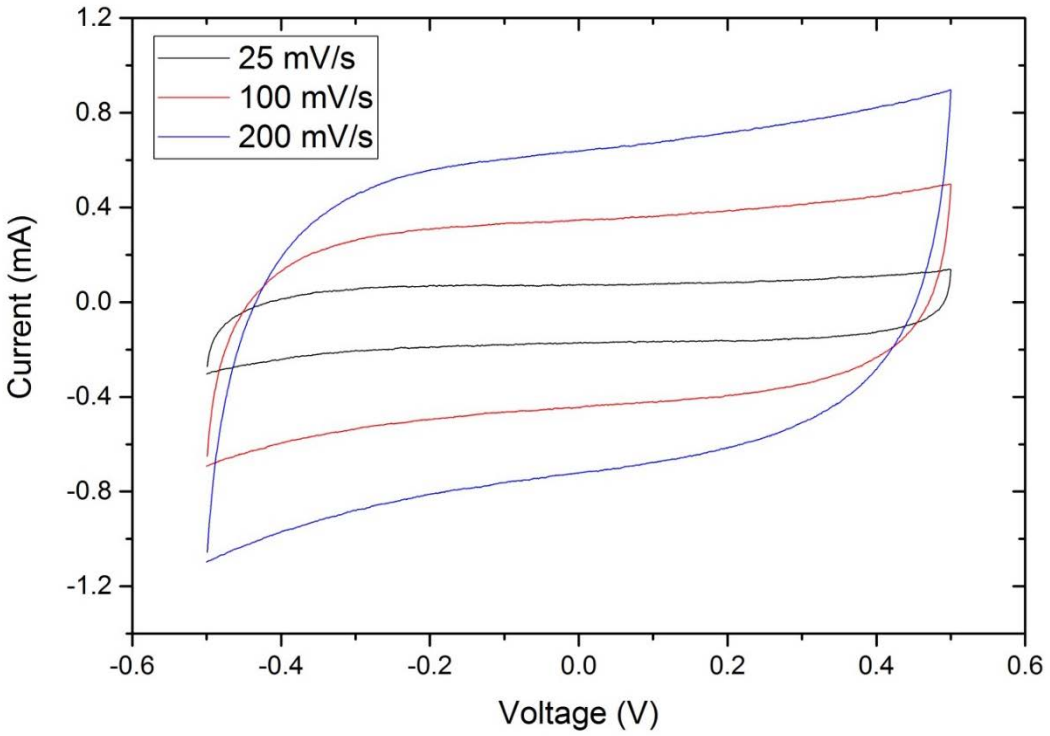

Fig. 11. Cyclic voltammetry curve for the KGP capacitors at different scan rates. a) capacitor/sensor 1, b) capacitor/sensor 2.

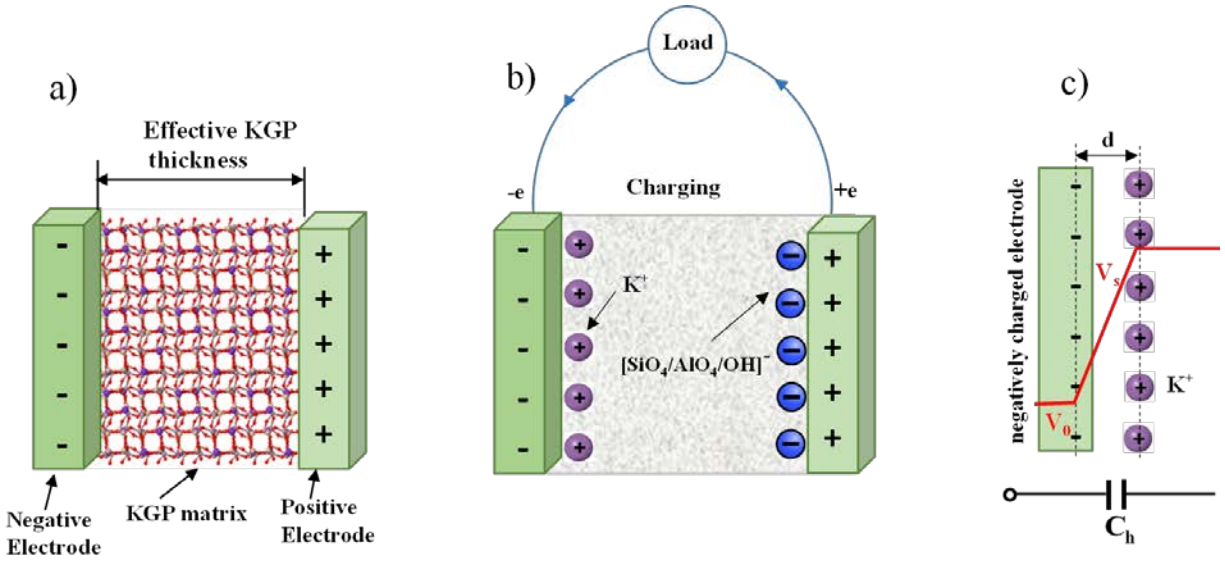

Fig. 12. Energy storage mechanism in the KGP capacitors. a) KGP capacitor, b) charging mechanism, c) formation of a double layer capacitor.

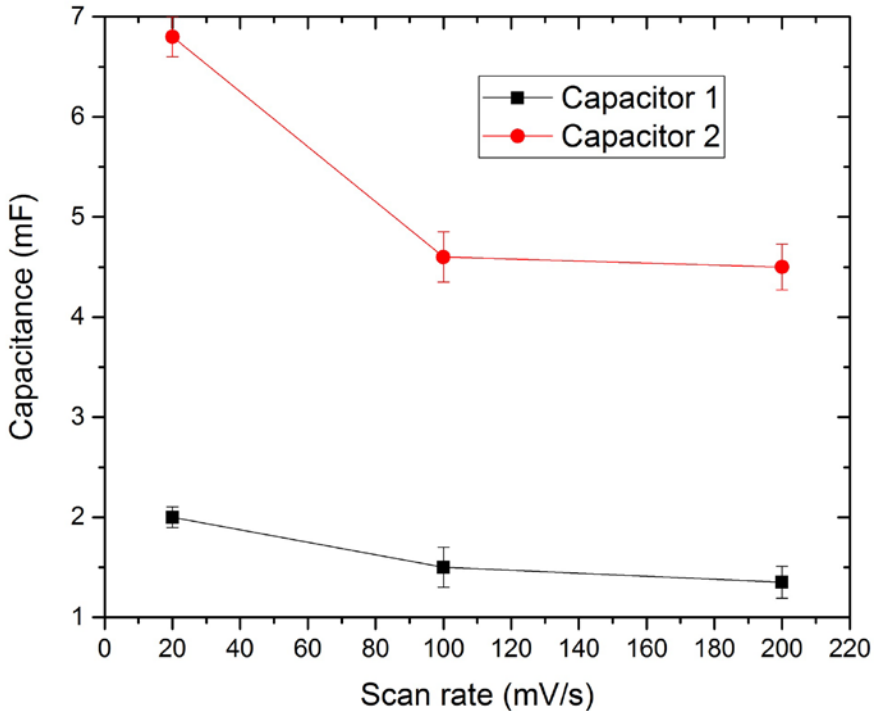

Fig. 13. Variation of the maximum capacitance of the KGP capacitors during charging as a function of the scan rate

a)

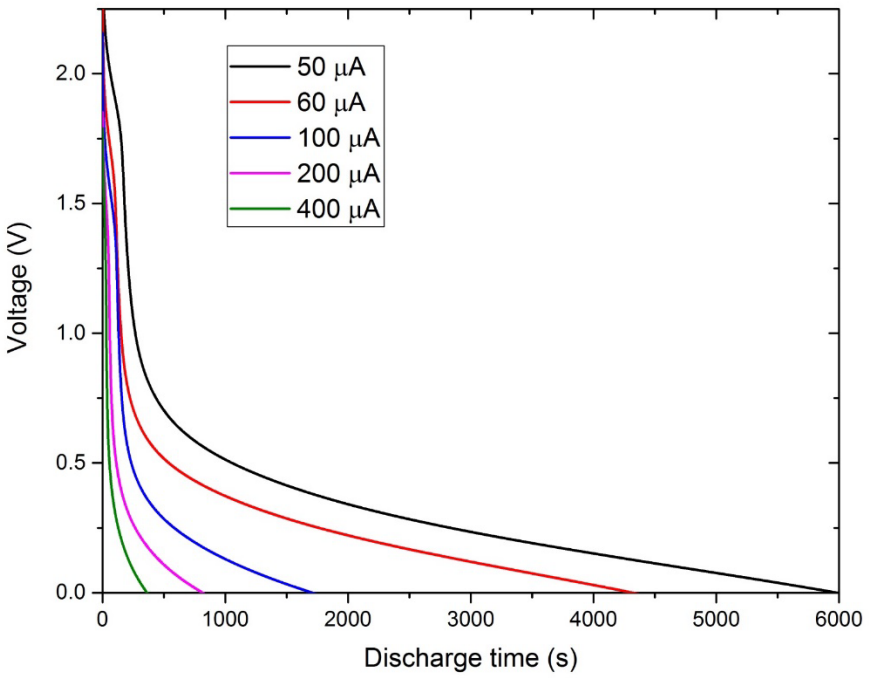

b)

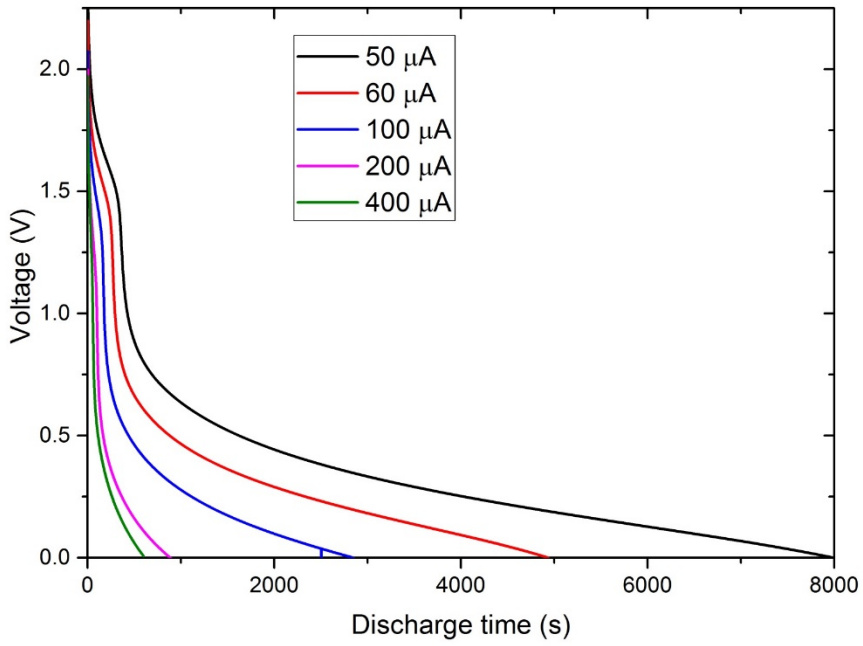

Fig. 14. Discharge behavior of the KGP capacitors at different discharge currents. a) capacitor 1, b) capacitor 2

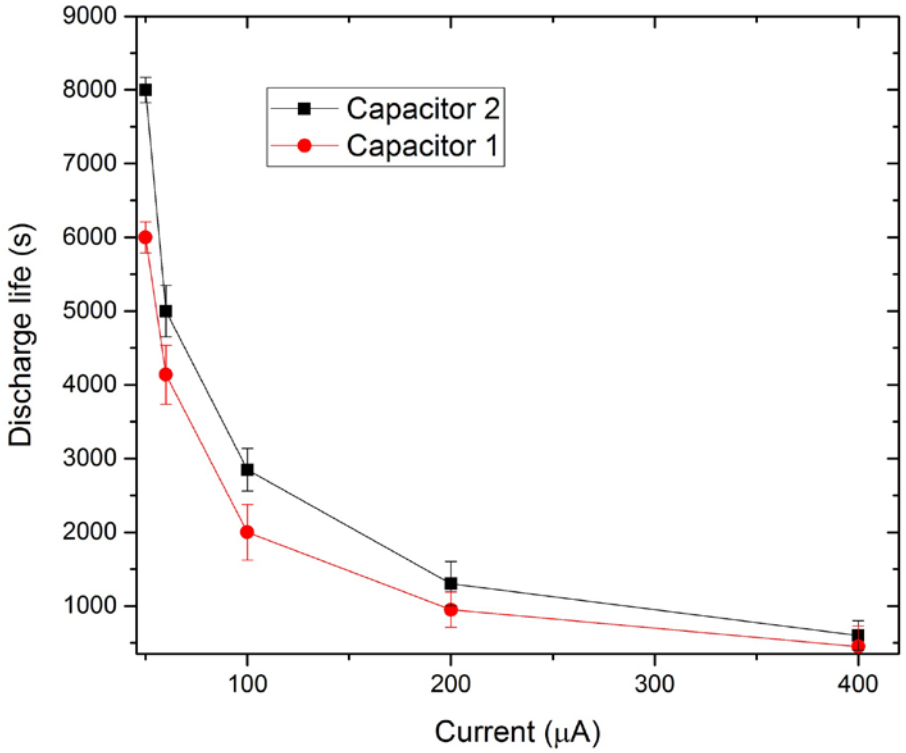

Fig. 15. Discharge life as a function of discharge current for the KGP capacitors

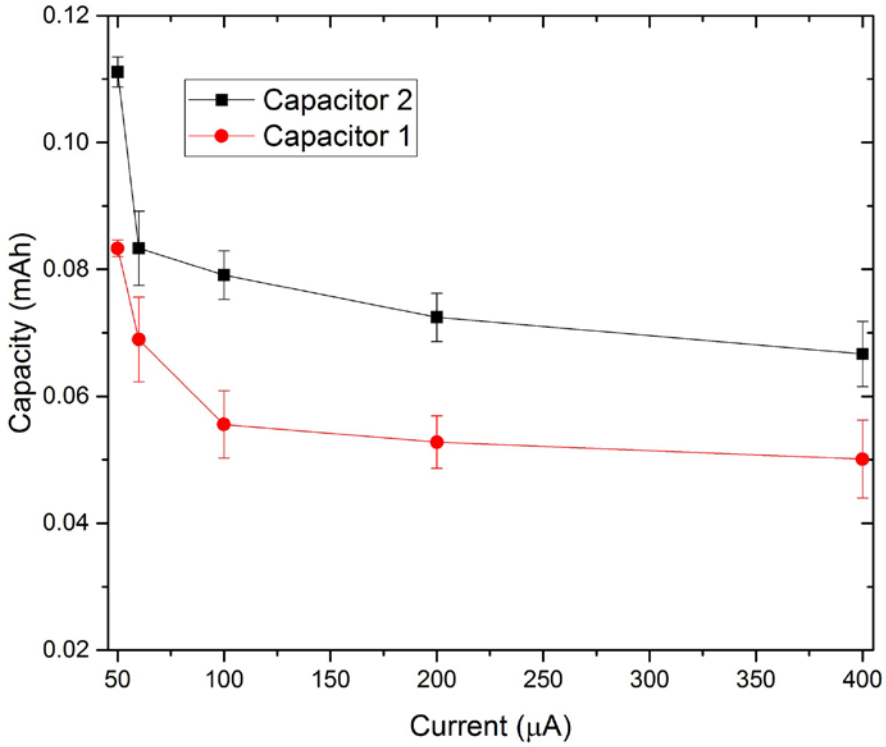

Fig. 16. Power capacity as a function of discharge current for the KGP capacitors

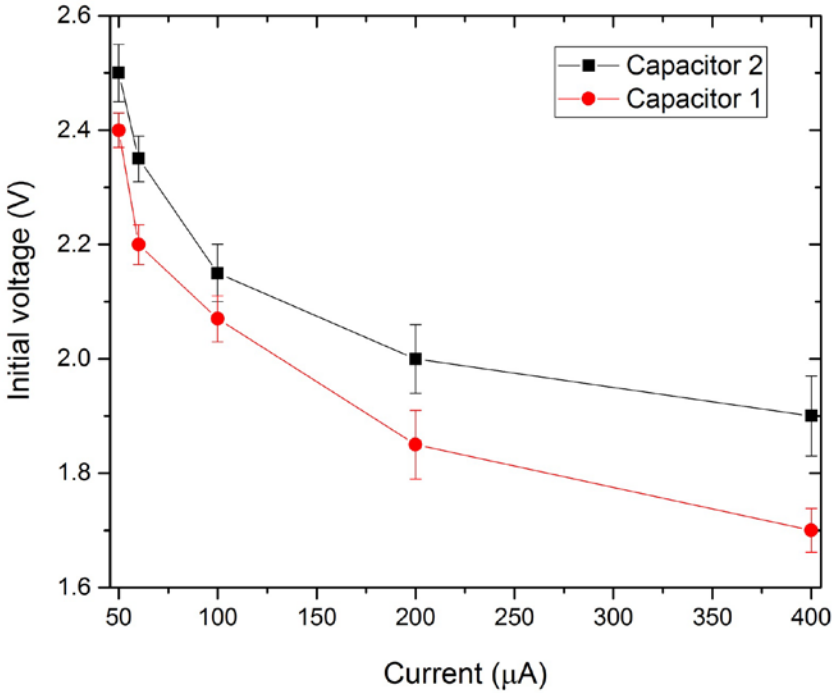

Fig. 17. Initial working voltage as a function of discharge current for the KGP capacitors

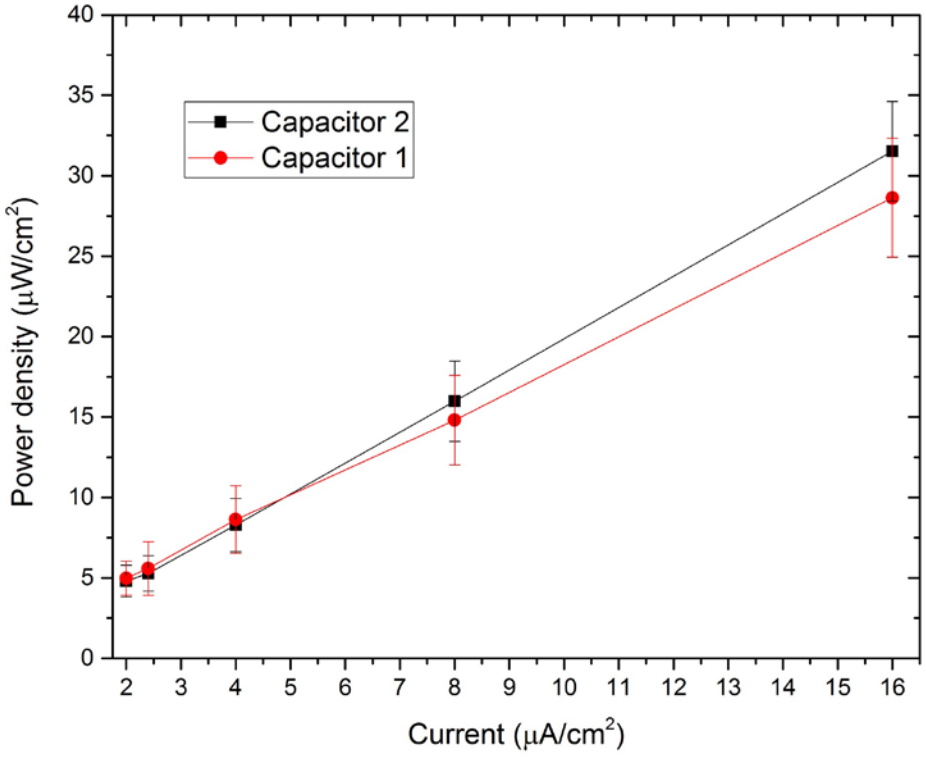

Fig. 18. Power density as a function of current density for the KGP capacitors

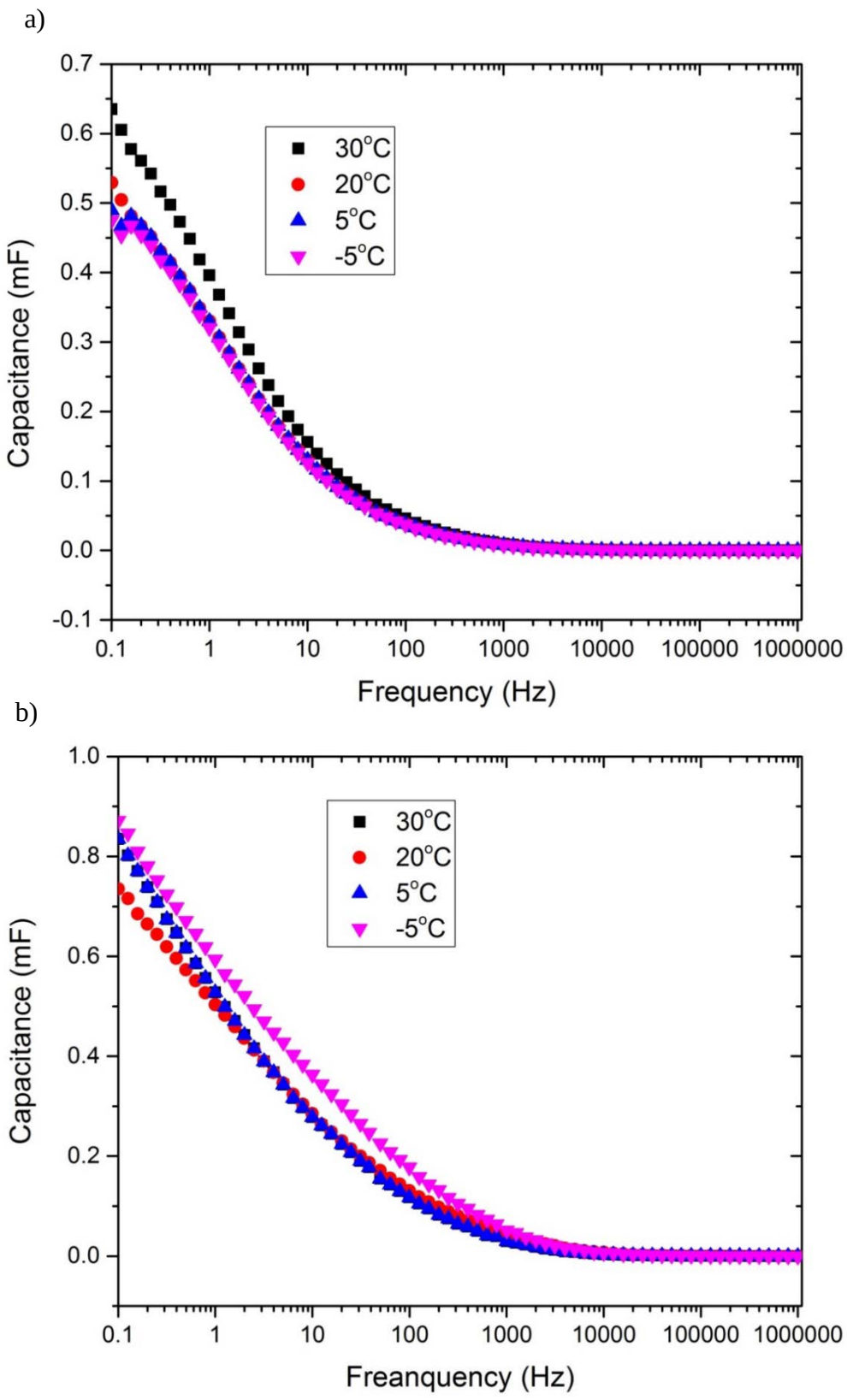

Fig. 19. Capacitance of the KGP capacitors/sensors at different temperatures. a) capacitor/sensor 1, b) capacitor/sensor 2

a)

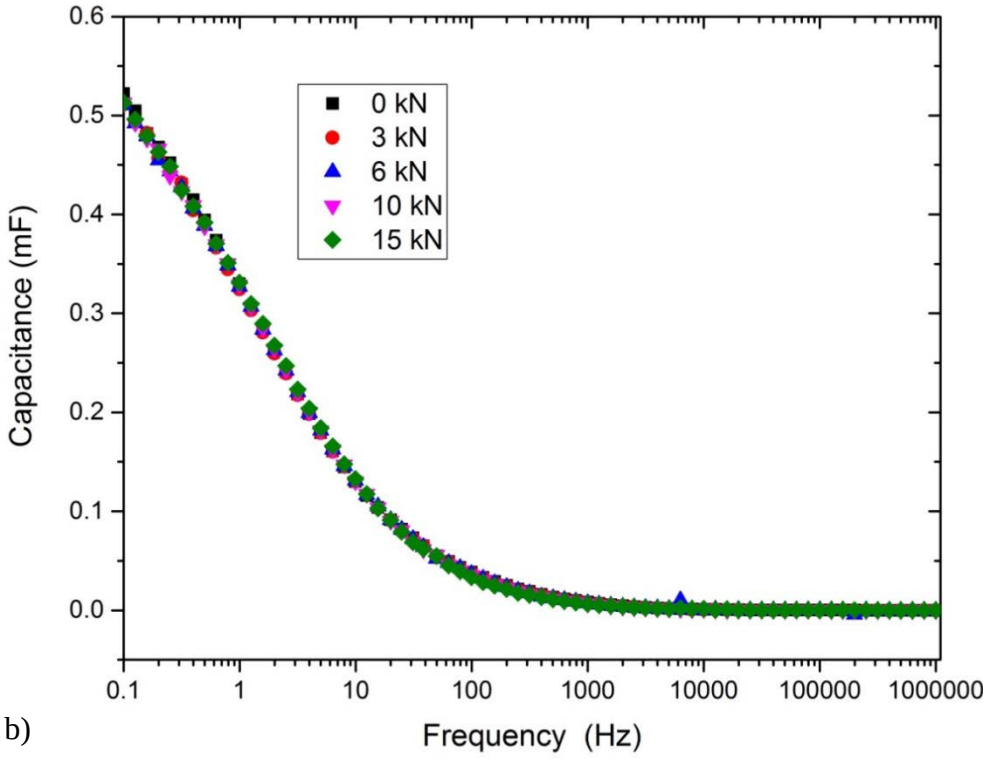

b)

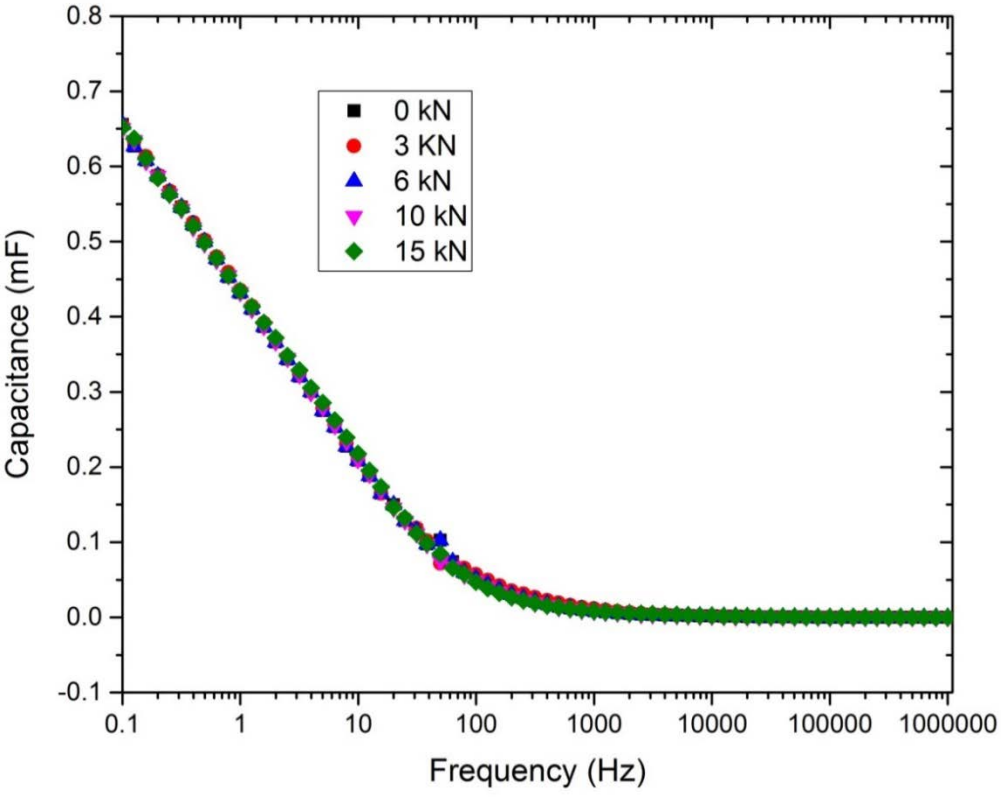

Fig. 20. Capacitance of the KGP capacitors/sensors at different loads. a) capacitor/sensor 1, b) capacitor/sensor 2

a)

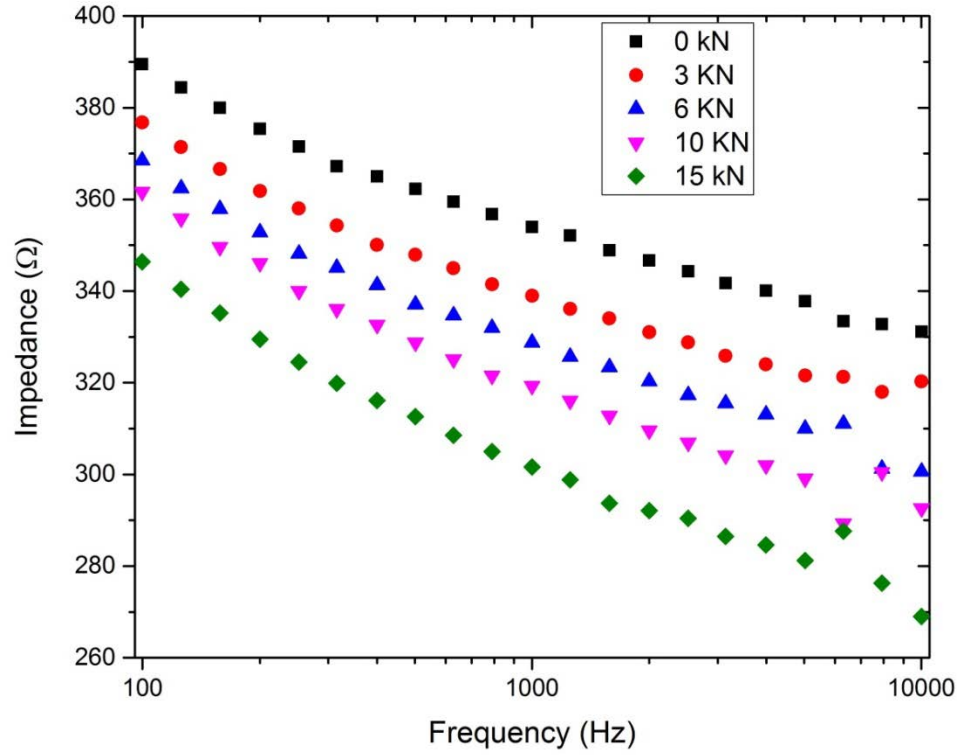

b)

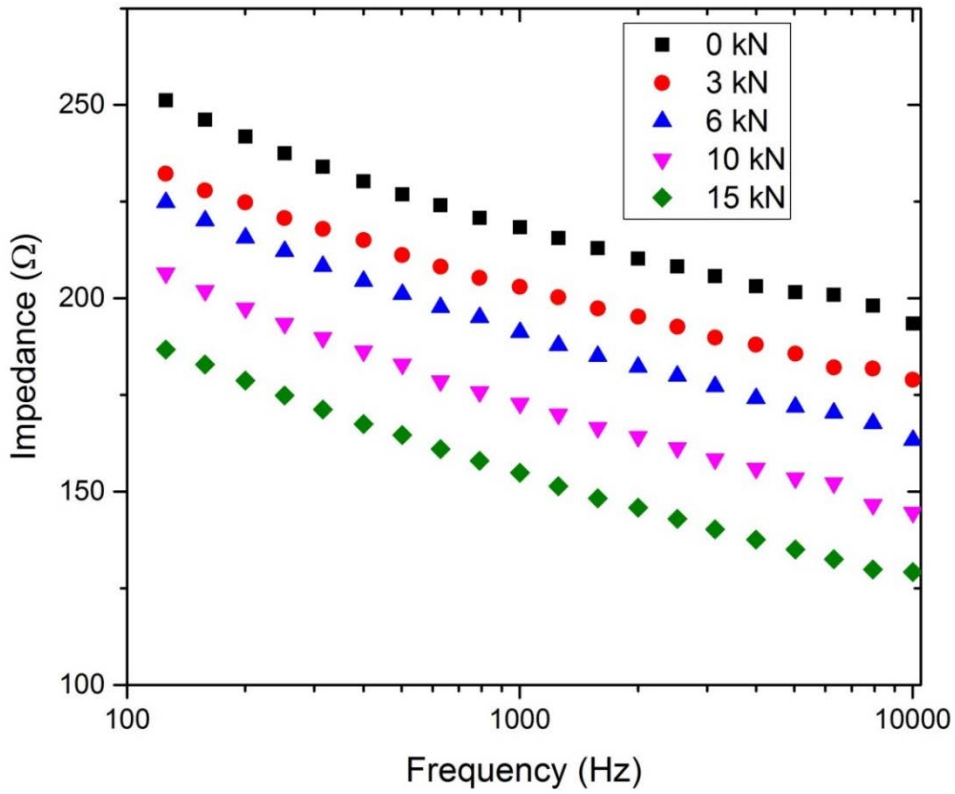

Fig. 21. Bod plots of impedance for KGP sensors at different loads. a) sensor 1, b) sensor 2

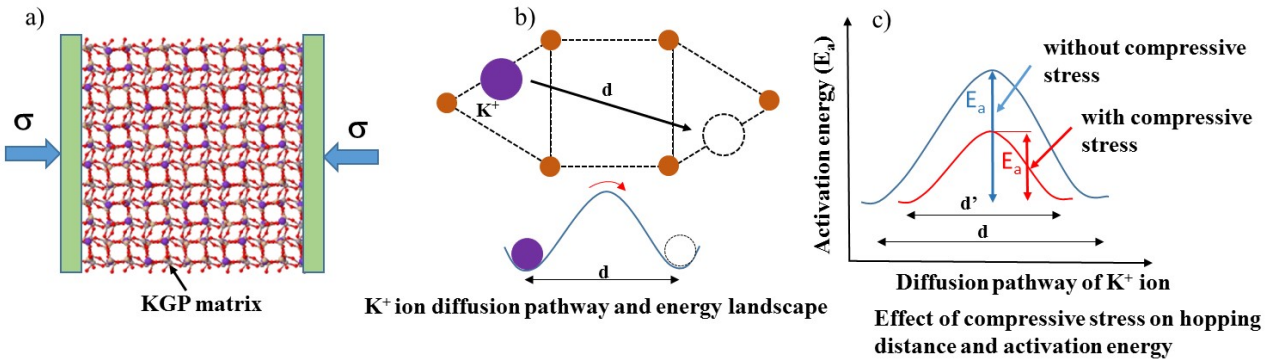

Fig. 22: Self-sensing mechanism of KGP cementitious composites. a) KGP sensor under stress, b) K^+ diffusion pathway in the KGP matrix and energy landscape, c) effect of the compressive stress on the activation energy and hopping distance *d*.

a)

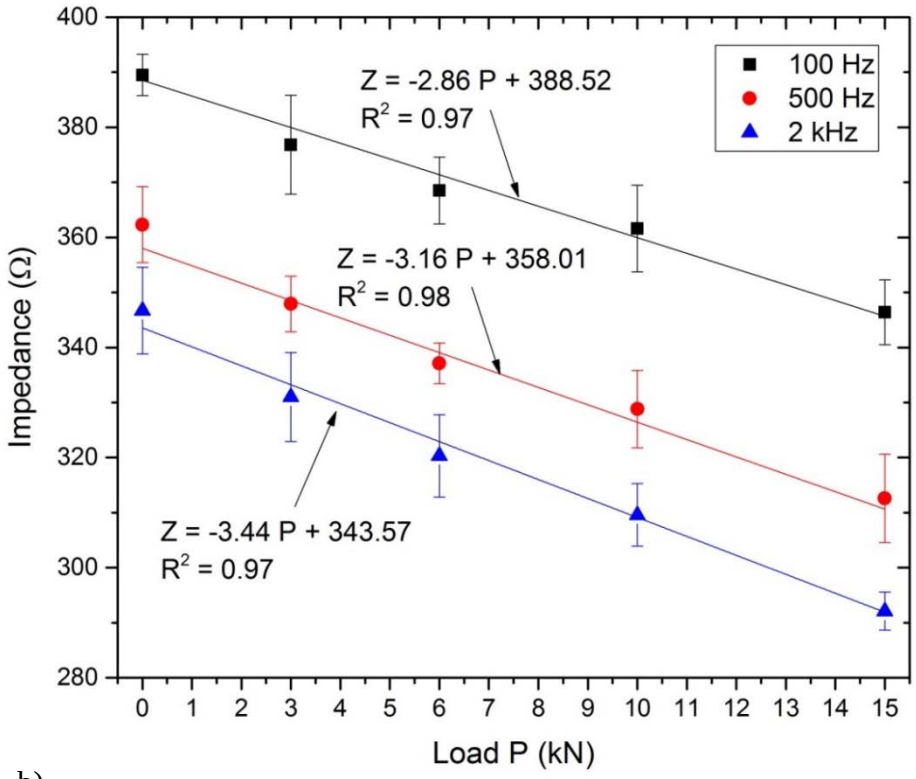

b)

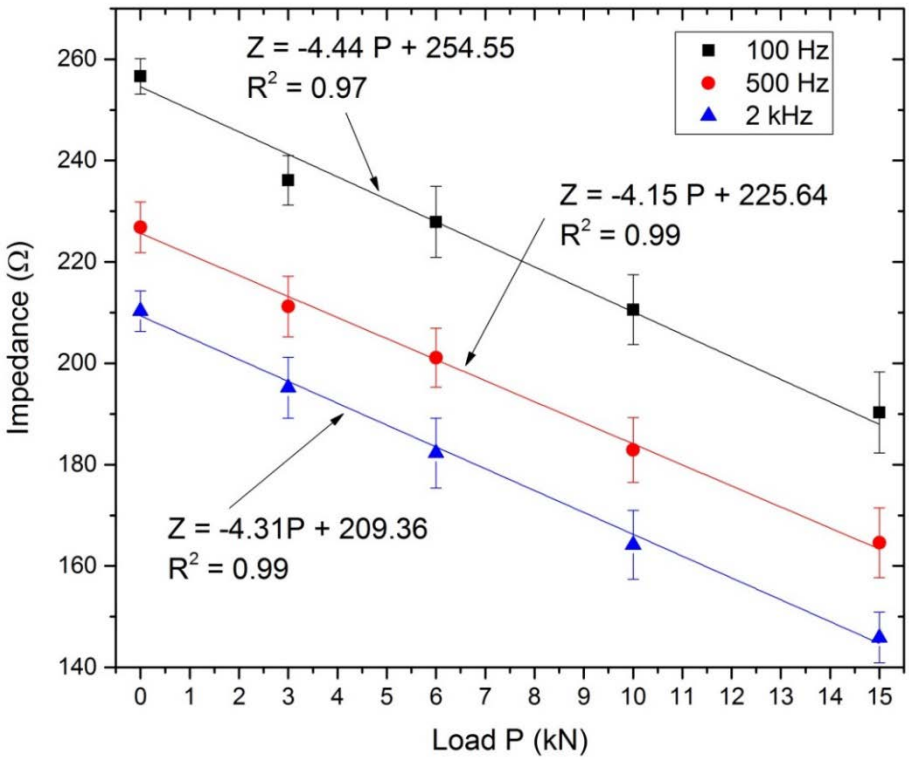

Fig. 23. Impedance of the KGP sensors as a function of load at different frequencies. a) sensor 1, b) sensor 2

a)

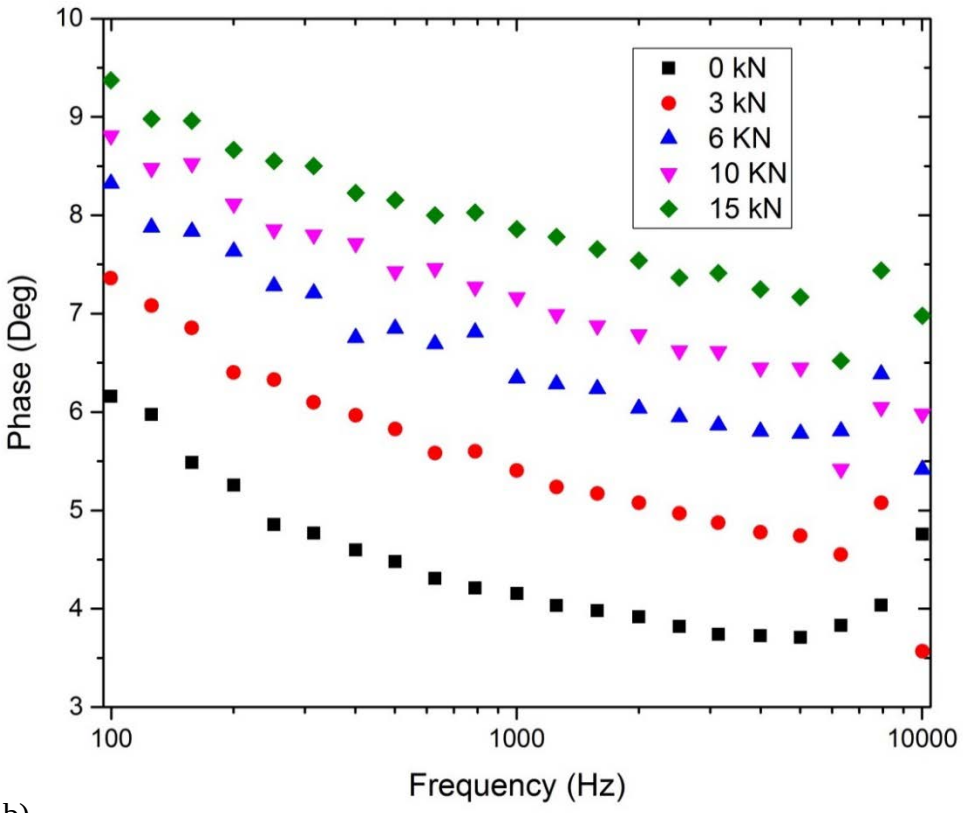

b)

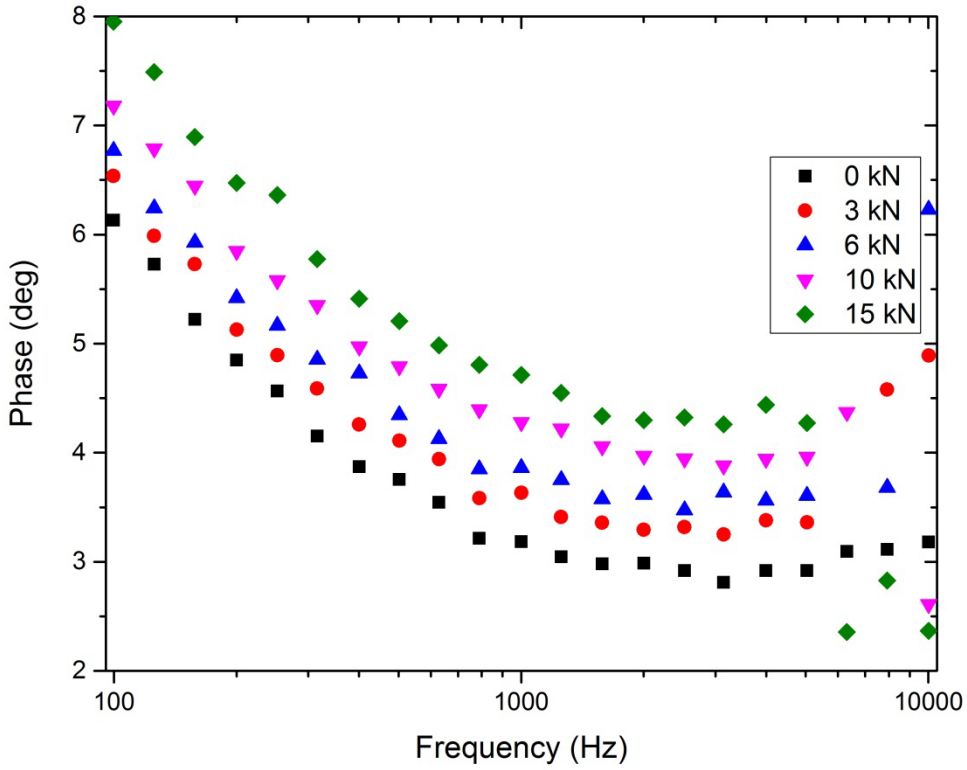

Fig. 24. Bod plots of phase for the KGP sensors at different loads. a) sensor 1, b) sensor 2

a)

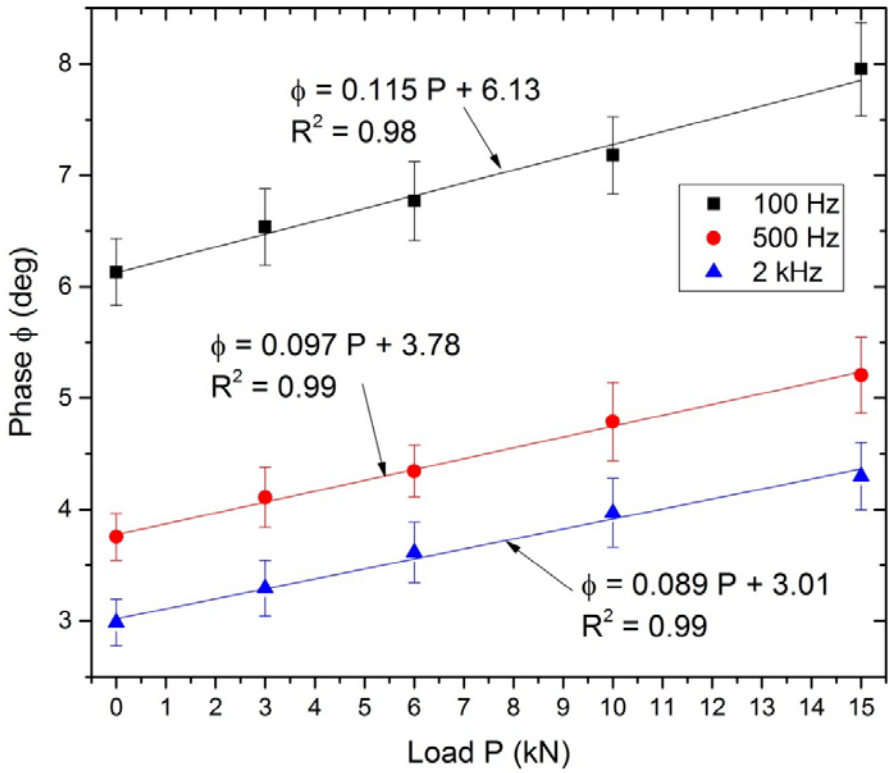

b)

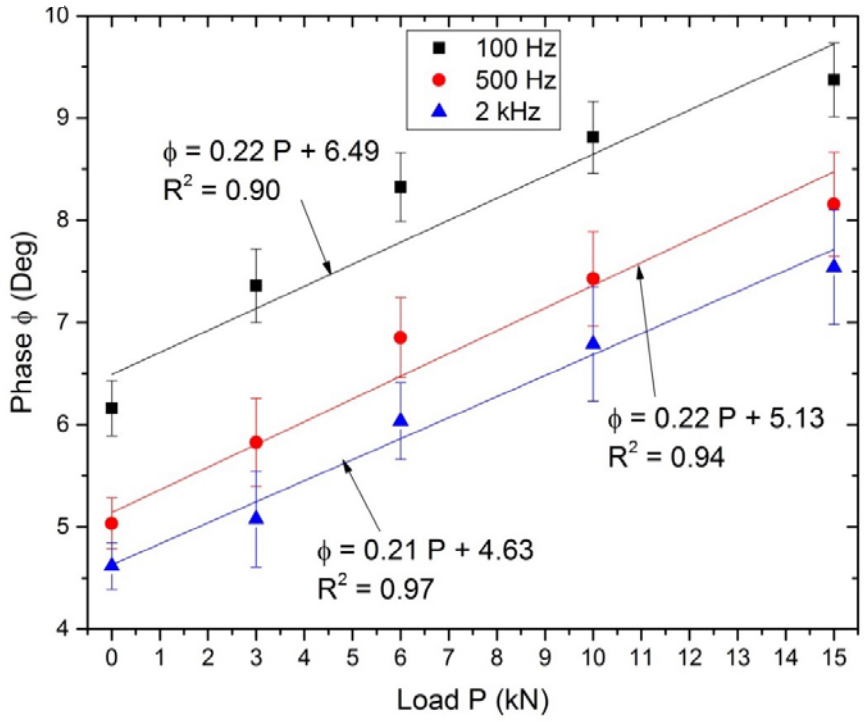

Fig. 25. Phase of the KGP sensors as a function of load at different frequencies. a) sensor 1, b) sensor 2